



RESEARCH ARTICLE | JANUARY 19 2024

Propulsive characteristics of single-pulsed jets with tube and orifice openings

Lei Gao (高磊) ; Xin Wang (王鑫); Simon C. M. Yu (余澄文) 



Physics of Fluids 36, 017124 (2024)

<https://doi.org/10.1063/5.0176021>



Articles You May Be Interested In

Physical understanding of gas-liquid annular flow and its transition to dispersed droplets

Physics of Fluids (July 2016)

An extended model for orifice starting jets

Physics of Fluids (June 2021)

On the asymptotic matching procedure predicting the formation number

Physics of Fluids (November 2021)



Physics of Fluids

Special Topics Open
for Submissions

[Learn More](#)

Propulsive characteristics of single-pulsed jets with tube and orifice openings

Cite as: Phys. Fluids **36**, 017124 (2024); doi: 10.1063/5.0176021

Submitted: 10 September 2023 · Accepted: 28 December 2023 ·

Published Online: 19 January 2024



View Online



Export Citation



CrossMark

Lei Gao (高磊),^{1,a)} Xin Wang (王鑫),² and Simon C. M. Yu (余澄文)³

AFFILIATIONS

¹School of Aeronautics and Astronautics, Sichuan University, Chengdu 610065, China

²Aviation University of Air Force, Changchun 130022, China

³Department of Aeronautical and Aviation Engineering, The Hong Kong Polytechnic University, Kowloon, Hong Kong, China

^{a)} Author to whom correspondence should be addressed: lei.gao@scu.edu.cn

ABSTRACT

The effects of the nozzle exit geometry on the unsteady propulsive characteristics of single-pulsed jets are studied numerically. For both tube and orifice nozzles, the jet exit configuration is parameterized by the diameter ratio R_D , which is defined as the ratio of the nozzle entrance D_0 to the jet exit diameters D . It is found that the diameter ratio has significant influence on the propulsive characteristics of the single-pulsed jet during its entire ejection phase. The total impulse production is augmented considerably as the diameter ratio increases until a critical value of $R_{D_crit} \approx 2.0$ is approached. The larger impulse production by the orifice nozzles over the tube nozzle stems from the persistent over-pressure contribution at the jet exit due largely to the fact that the flow contraction near the jet exit of the orifice nozzle results in the intensification of the radial velocity gradients and higher local pressure. By using the existing prediction of the contraction coefficient C_c to account for the flow contraction, a theoretical model has been developed with the quasi-one-dimensional flow approximation to predict the pressure thrust at the jet exit during the steady discharging stage, showing good agreement with the present numerical results. Moreover, the pressure force acting on the vertical wall of the orifice nozzle, which is proportional to the wall area, is found to be primarily responsible for the larger transient variations in the jet impulse during the onset and end of the jet ejection phase as the diameter ratio increases.

Published under an exclusive license by AIP Publishing. <https://doi.org/10.1063/5.0176021>

I. INTRODUCTION

It is well known that the unsteady pulsed jet generated by ejecting fluid intermittently and periodically into the surroundings is efficient for underwater propulsion.^{1–4} This serves as the basic mechanism for locomotion of several marine organisms such as jellyfish,^{5,6} squid,^{7,8} and salp.⁹ In addition to the recent progress in the understanding of the swimming theory of fishes by undulation and the flying theory of birds and insects by flapping, bio-inspired propulsion by means of the pulsed jet has gradually become an intriguing subject for researchers due to its advantages in augmenting the thrust generation and improving propulsive efficiency.^{10–13}

Unlike the steady continuous jets, the unsteady pulsed jet is generically characterized by the formation and development of large-scale coherent vortices via the roll-up of the shear layer separated from the jet exit. The investigation in the formation and evolution of the vortex ring produced by the single-pulsed jet with finite fluid discharged (or commonly known as starting jet) occupies a substantial volume of the previous literature.^{14–17} These studies on the characteristics of the vortex dynamics in the starting jet provide the theoretical

basis for its application in the bio-inspired jet propulsion devices. It has been demonstrated that the starting jet would generate greater thrust than the corresponding steady jet at the same Reynolds number.^{3,18,19} Krueger and Ghairb¹⁸ suggested that enhanced impulse and thrust generation by a starting jet originates from the nozzle exit over-pressure, which, in turn, serves to accelerate the ambient quiescent fluid associated with the vortex ring formation in the forms of the added mass and entrained fluids. Ruiz *et al.*¹⁹ extended the previous results for the stationary jet nozzles to a self-propelled vehicle, showing that, at Reynolds number of 6000, vortex-enhanced propulsion can yield up to a 50% increase in the propulsive efficiency over a steady jet. Subsequently, the study of Whittlesey and Dabiri³ found that the maximum propulsive efficiency can be achieved when the leading vortex ring starts to pinch off from its trailing jet, within a higher Reynolds number range of $Re = 9 \times 10^4 \sim 1 \times 10^6$. Therefore, the aforementioned results suggest that the propulsive performance enhancement of the starting jet is closely related to the nozzle exit over-pressure and the dynamics of the vortical structures in its near wake.

In the study of the single-pulsed jet and the associated vortex ring formation, the piston-cylinder apparatus is usually adopted as the jet generator. Two typical configurations of this jet generator are the tube and orifice nozzles, as illustrated schematically in Fig. 1. For the orifice nozzle configuration, the opening is a hole on a vertical wall plane, whereas for the tube nozzle configuration, the jet exit is protruding into the surrounding flow field. The orifice geometry forces the flow to contract as it approaches the exit, which, in turn, strongly affects the boundary conditions at the jet exit, i.e., the axial and radial velocity profiles as well as the vorticity flux carried by the separated shear layer. The typical tube and orifice nozzle configurations can be parameterized in terms of a dimensionless diameter ratio R_D , which is defined as the ratio of the nozzle diameter D_0 to the jet exit diameter D , with $R_D = 1$ for the tube nozzle and $R_D > 1$ for the orifice nozzle, as shown schematically in Fig. 1. It is worth mentioning that, in addition to the classic piston-cylinder configuration for the mechanical jet generator, the unsteady jet could also be produced by the large-amplitude self-excited oscillations of collapsible channel upstream of the jet exit.^{3,20}

The previous studies related to the jet exit geometry mainly focused on the difference in circulation production and vortex dynamics between the tube and orifice nozzle configurations. The influence of the nozzle exit geometry on the formation of vortex rings was first examined by Pullin,²¹ who derived an analytical model for the vortex circulation and vortex core trajectories for both tube and orifice nozzles based on the similarity theory. By taking into account the effect of jet exit over-pressure, Krueger^{22,23} theoretically predicted the jet circulation generated by both the tube and orifice configurations. They found that the orifice nozzle produces more circulation than the tube nozzle, due to the effect of flow contraction at the orifice nozzle exit. Rosenfeld *et al.*²⁴ later studied the transient development of the jet circulation issuing from a converging nozzle with various cone angles, in which the orifice case is regarded as the limiting case of 90° angle, and showed that the radial velocity contribution to the circulation production is not limited to the impulsive initiation of the jet only but persists the entire duration of the jet ejection. The existing investigations demonstrated that both total circulation and the development of the vortex ring can be manipulated to some extent by the geometry of the jet exit.

However, there are only a few studies discussing the influence of jet exit configuration on the impulse and thrust generation by the single-pulsed jet, which would be of great interest in the applications related to the biological and engineering propulsion systems. Recently, Krieg and Mohseni²⁵ studied the dynamic properties (i.e., the circulation, hydrodynamic impulse, and kinetic energy) of starting jets produced by the two jet configurations. It was found that higher radial velocity component produced by the converging streamlines at the jet exit of the orifice nozzle would lead to 75% more impulse than that by

the tube nozzle under the equivalent generation conditions. Most recently, Limbourg and Nedić²⁶ investigated experimentally the formation process of vortex rings formed with an orifice nozzle generator with the jet stroke-to-diameter ratio being the key parameter. Similar to the previous results,²⁵ the production of the total dynamic properties was observed to be significantly increased by the orifice nozzle. Moreover, by employing the same experimental apparatus,²⁶ Limbourg and Nedić^{27,28} conducted a comprehensive parametric study of the effects of the diameter ratio on the final production of the dynamic properties of the starting flow. Based on the theoretical estimation of the contraction coefficient of the orifice nozzle generator, they proposed a modified slug-flow model to satisfactorily account for the contraction effect imposed to the flow by the orifice plate at the jet exit. It is noted that, in their experimental setup, the change in the diameter ratio is realized by changing the exit diameter D while keeping the nozzle diameter D_0 constant. Consequently, their conclusion²⁷ made for the fixed jet exit velocity scenario that a maximum in the production rate of impulse and energy at large time can be identified at a diameter ratio of about 1.11 is compromised by simultaneous variation in diameter ratio and Reynolds number.

To sum up, these previous studies mainly focus on the significance of non-zero radial velocity at the exit of the static orifice nozzle on the generation of dynamic properties, in order to clarify its influence on the formation dynamics of the vortex ring. Therefore, the diameter ratio has yet been considered as the independent parameter for the study of the propulsive performance of the single-pulsed jet, and the physical mechanisms underlying its effects on the jet impulse generation have not been fully understood. In the present study, we investigate numerically and theoretically the effects of the jet exit geometric configuration on the propulsive characteristics of the single-pulsed jet, intending to identify the primary factors affecting the jet impulse and thrust generation as well as to provide some insight into its application in the aquatic propulsion devices. This paper is organized as follows. Section II describes the computational method and physical model of the single-pulsed jet discharging from both tube- and orifice-nozzle configurations. Section III presents the results of the propulsive quantities of the total jets with different diameter ratio and explains the evolution of propulsive characteristics in terms of a control volume analysis in its near wake. Finally, a simple empirical formula to describe the effects of diameter ratio to the total jet impulse production is proposed. This paper ends with brief concluding remarks in Sec. IV.

II. NUMERICAL METHOD AND VALIDATION

The single-pulsed jets generated by the piston-cylinder apparatus are simulated in the rectangular domain on the x - r plane with

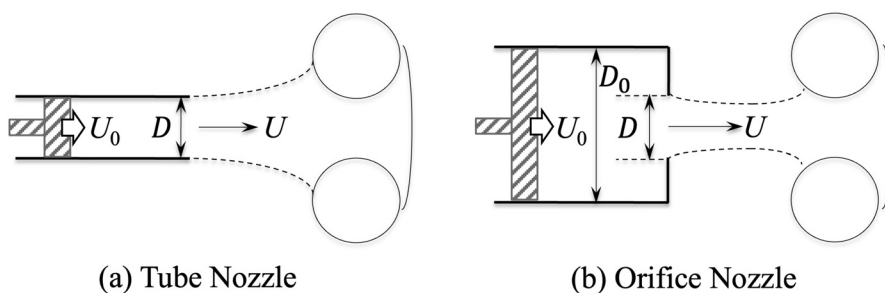


FIG. 1. Schematic of (a) tube nozzle and (b) orifice nozzle configurations of piston-cylinder apparatus for the jet generator.

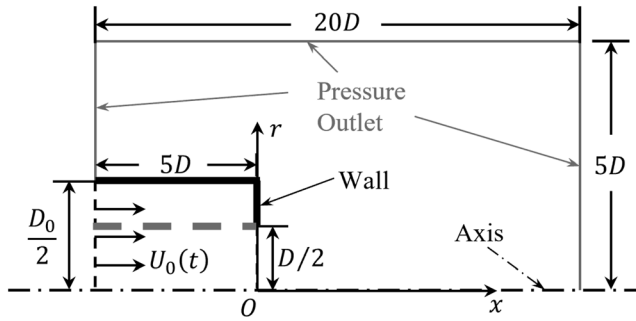


FIG. 2. Computational domain and boundary conditions used in the numerical simulation of the single-pulsed jets with tube nozzle (indicated by the thick gray dashed lines) and orifice nozzle configurations (indicated by the thick black solid lines). Note that the sketches are not drawn in scale.

different nozzle wall geometry as shown in Fig. 2. To quantitatively compare the starting flows generated by the two types of jet generator, the nozzle exit diameter is taken as the length scale and was kept constant at $D = 0.02$ m for all cases in the present study. Limbourg and Nedić²⁷ investigated the effect of diameter ratio of the orifice nozzle in their experimental study by keeping the nozzle diameter D_0 constant while changing the orifice exit diameter D . In this way, Reynolds number of the jet would change simultaneously with the diameter ratio, making these two non-dimensional parameters coupled. By using numerical simulation, the present study can easily isolate the effect of the diameter ratio from the jet Reynolds number by keeping the jet exit diameter fixed while changing the nozzle diameter.

The computational domain has a dimension of $20D$ in the axial direction and $5D$ in the radial direction from the axis of symmetry, which had been found to be sufficiently large to ensure that the outer boundary conditions do not influence the dynamics of the flow evolution.^{23,29} The flow inside the jet nozzles is also simulated here by setting their axial length equal to $5D$ and their diameter equal to the nozzle diameter D_0 , as shown in Fig. 2. The wall of the tube and orifice nozzles, as well as the vertical wall of the orifice nozzle at the exit plane, were modeled in the domain by zero-thickness virtual walls with the non-slip boundary condition imposed on. The motion of the piston was simulated by specifying a uniform velocity profile of U_0 on the nozzle entrance boundary (i.e., $x/D = -5$ and $0 < r/D_0 < 0.5$) by the velocity inlet boundary condition. On the outer and downstream boundaries, the pressure outlet is specified, and flow entrainment is allowed. The nozzle centerline is taken as the axis of symmetry.

At time $t = 0$, the flow over the whole computational domain is assumed to be at rest. Immediately after the jet initiation, a jet exit velocity program $U(t)$, which is given by

$$\frac{U(t)}{U_{\max}} = \begin{cases} \frac{t}{T_1} - \frac{1}{2\pi} \sin \frac{2\pi t}{T_1} & (t \leq T_1), \\ 1 & (T_1 < t \leq T_0 - T_1), \\ \frac{T_0 - t}{T_1} + \frac{1}{2\pi} \sin \left[\frac{2\pi}{T_1} (t - T_0 + T_1) \right] & (T_0 - T_1 < t \leq T_0), \\ 0 & (t > T_0), \end{cases} \quad (1)$$

is specified at the nozzle velocity exit boundary (i.e., $x/D = 0$ and $0 < r/D < 0.5$), where T_1 is the acceleration and deceleration period

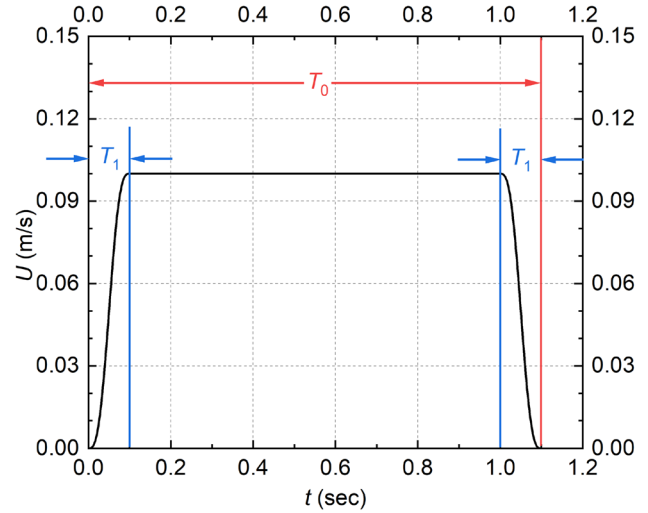


FIG. 3. Jet exit velocity programs $U(t)$ used to generate the single-pulsed jets.

of the jet velocity, T_0 is the total jet period, and U_{\max} is the maximum jet velocity. With the focus on the effect of nozzle geometric configuration on the jet propulsive characteristics, a typical velocity program is adopted for all the cases studied herein with $U_{\max} = 0.1$ m/s and equal acceleration and deceleration periods, as illustrated in Fig. 3. The velocity program is exactly the same as the fast acceleration and deceleration (FAD) type of the velocity program adopted in Gao *et al.*,³⁰ which is found to achieve the largest total jet impulse for the same stroke ratio and Reynolds number. To model the single-pulsed jet issued from different nozzle exit configurations, seven cases with diameter ratio R_D ranging from 1 to 4 have been investigated. Accordingly, the flow velocity at the nozzle entrance can be determined from the conservation of mass as $U_0(t) = (D/D_0)^2 U(t)$. Based on the jet velocity program and jet exit diameter, the dimensionless stroke-length to diameter ratio, defined as $L/D = (\int_0^{T_0} U(t) dt)/D$, is also kept constant at $L/D = 5$, which is greater the critical stroke ratio of around 4 found by Gharib *et al.*¹⁷ Therefore, the vortex ring pinch-off process can be observed in the present study. In addition to the stroke ratio, the Reynolds number of the starting jet, defined as $Re = (U_{\max} D)\nu$, where ν is the fluid kinematic viscosity, has also been taken as constant value of 2000 for all simulations. Table I summarizes the flow parameters for different cases in the present study.

TABLE I. Flow parameters for the single-pulsed jet with tube nozzle and orifice nozzle configurations.

Case	$R_D = D_0/D$	D_0 (cm)	$U_{0,\max}$ (m/s)	U_{\max} (m/s)
T1	1.0	2	0.1000	0.1
O1	1.2	2.4	0.0694	0.1
O2	1.5	3	0.0444	0.1
O3	2.0	4	0.0250	0.1
O4	2.5	5	0.0160	0.1
O5	3.0	6	0.0111	0.1
O6	4.0	8	0.0063	0.1

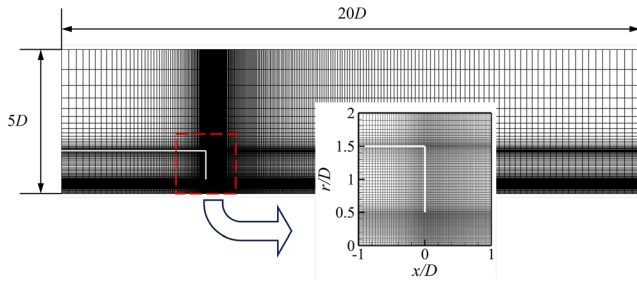


FIG. 4. Sample mesh used for the orifice case O_3 with $R_D = 3$. The thick white lines indicate the orifice wall boundaries. Totally, 599×179 nodes were used in the axial and radial directions. Only every second mesh point is shown.

The flow development is simulated using the axisymmetric, unsteady, incompressible, and laminar Navier–Stokes equations. The governing equations are solved by the finite volume technique in the computational fluid dynamics package ANSYS Fluent, with the PISO algorithm for pressure-velocity coupling. A second-order implicit scheme is used for temporal and spatial integration. The domain is discretized using a non-uniform, structure grid with 599×179 nodes in the axial and radial directions, respectively, as illustrated in Fig. 4. A total of 106, 444 quadrilateral cells are utilized, which are refined toward the jet exit and shear layer regions (i.e., $x/D = 0$ and $r/D = 0.5$), as well as the nozzle wall boundaries (i.e., $r/D = D_0/D$) so as to resolve the areas of large velocity gradients both inside and outside the nozzle. In order to test the grid independence, case O_3 is simulated with three grids with nodal dimensions of 399×119 , 599×179 , and 899×269 . Comparing the hydrodynamic impulse I_h [which is defined by Eq. (2) in Sec. III A] at the jet termination (at $t = 3$ s) for three cases gave 0.48% relative difference between the 599×179 and 899×269 grids, while the 399×119 grid provided 4.72% difference in I_h relative to that for the 599×179 grid. Moreover, the axial velocity profiles at the jet exit plane obtained by the three grids are presented and compared in Fig. 5 for two typical instants during the jet development. As shown, the 599×179 and 899×269 grids offer converged data of the velocity profiles within the shear layer

region ($0.45 < r/D < 0.5$), relative to the coarser 399×119 grid. Thus, the 599×179 grid is used in the present simulation. The hydrodynamic impulse is also calculated using several dimensionless time steps $\Delta t^* = (U_{\max} \Delta t)/D = 0.0025, 0.005, 0.025$. The difference between the two smallest time steps is lower than 0.3%, and, therefore, a constant time step $\Delta t^* = 0.005$ is selected for the present numerical study.

By using the current numerical method, we also compare quantitatively the circulation and hydrodynamic impulse of the total jet with experimental measurements of Limbourg and Nedić.²⁷ The results are plotted in Fig. 6. It can be seen that the results of the current method agree reasonably well with the experimental measurement.²⁷ From these results, we can conclude that the current simulation is capable of obtaining reliable results for the dynamics of the jet flow, especially for the production of integrals of motion in the near field.

III. RESULTS AND DISCUSSION

A. Evolution of propulsive quantities in the single-pulsed jet

The effects of nozzle exit geometry on the propulsive performance of the single-pulsed jet are examined first in terms of the hydrodynamic impulse delivered to its near wake. For the axisymmetric flows, the hydrodynamic impulse I_h can be calculated as

$$I_h = \pi \rho \int \omega r^2 dx dr, \quad (2)$$

where ω is the azimuthal component of the vorticity. The integration is carried out over the domain outside of the jet nozzle, consisting of both upstream (i.e., $x/D < 0$ and $r/D_0 > 0.5$) and downstream (i.e., $x/D > 0$) regions. It is noted that the hydrodynamic impulse can be considered as the total mechanical impulse required to generate the flow from rest.

The evolution of the hydrodynamic impulse, normalized as $I_h^* = I_h / (\pi \rho D^3 U_{\max})$, against the formation time t^* ($t^* = \overline{U}(t)t/D$, where $\overline{U}(t)$ is the running average of the jet exit velocity) for the cases with different diameter ratios is shown in Fig. 7. The theoretical results of the slug model,^{16,31} which assume that the fluid is ejected through the jet exit with a uniform axial velocity and no radial velocity, are also

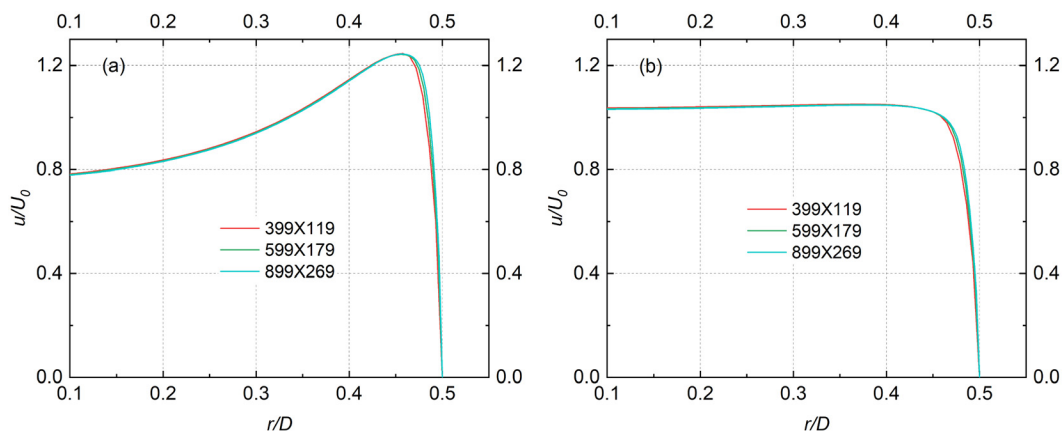


FIG. 5. The axial velocity profiles $u(r)$ at the jet exit plane for the case O_3 obtained by the three grid sizes. (a) During the initial acceleration stage $t^* = 0.25$ and (b) at the end of the steady discharging stage $t^* = 4.75$.

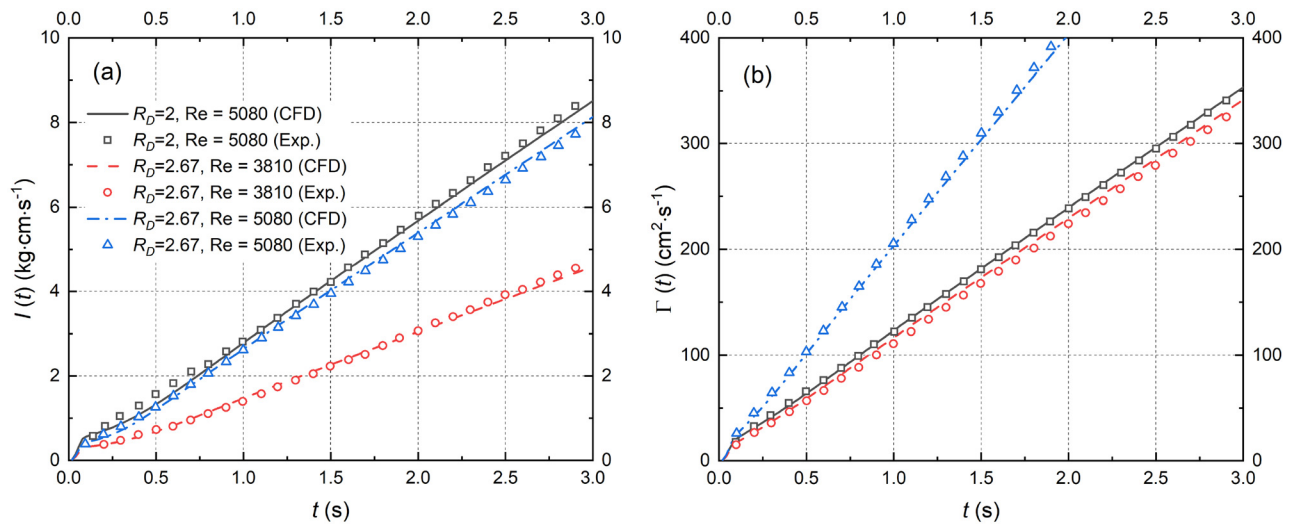


FIG. 6. Comparison of the present numerical results with the experimental results of Limbourg and Nedić.²⁷ (a) The hydrodynamic impulse and (b) the circulation.

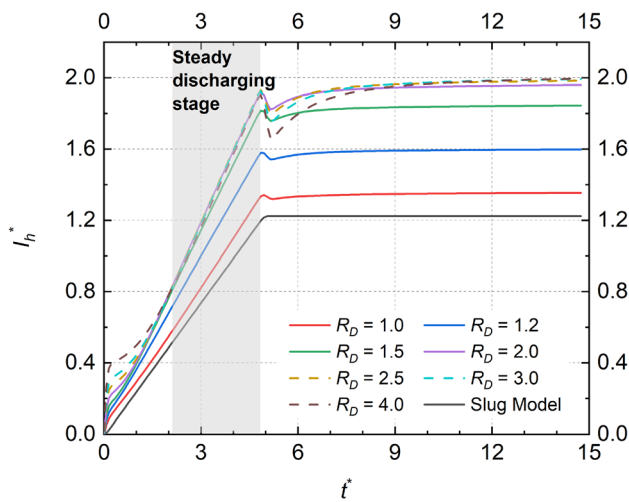


FIG. 7. Evolution of the hydrodynamic impulse for the single-pulsed jets with different diameter ratios.

included for comparison. In general, the hydrodynamic impulse production is found to be enhanced as the diameter ratio increases from $R_D = 1$ for the tube nozzle to $R_D = 4$ for the orifice nozzle. During the steadily discharging stage in which I_h^* grows almost linearly with t^* (i.e., approximately during $2 \leq t^* \leq 5$, as highlighted by the gray region in Fig. 7), the rate of impulse growth becomes larger with the increase in the diameter ratio. As a result, the total hydrodynamic impulse delivered by a single jet pulse is boosted by the diameter ratio, especially in the range of $1 \leq R_D \leq 2$. At about $t^* = 15$, the hydrodynamic impulse for the case $R_D = 2$ is found to be approximately 44.6% greater than that for the tube case. However, as R_D continues to rise from 2 to 4 in the orifice nozzle regime, the increase in total hydrodynamic impulse is merely 1.8%, indicating that an asymptotic state of impulse enhancement is approached beyond $R_D = 2$. In other words,

a further increase in the diameter ratio beyond a critical value of $R_{D_cir} \approx 2$ would play a negligible role in the jet impulse production for a single jet pulse. The asymptotic influence of the diameter ratio can also be revealed qualitatively by the flow structure evolution results, as shown in Fig. 8. Even though the general flow patterns are similar for both tube- and orifice-nozzle cases, the streamwise translation of the leading vortex ring becomes faster as the diameter ratio increases until $R_D = 2$ is approached. It can be seen in Fig. 8 that the difference in the vortical structures cannot be discern between the $R_D = 2$ case and $R_D = 2.5$ case. The experimental study of Krieg and Mohseni²⁵ also found that the orifice opening cases with the stroke ratios of $L/D = 2.4$ and 7 were capable of producing hydrodynamic impulse about 74% higher than the tube nozzle configuration under the same conditions, which is slightly higher than the enhancement of 64% in hydrodynamic impulse found in the present cases. Based on the discussion earlier, we may, therefore, identify a critical diameter ratio $R_{D_cir} \approx 2$ for the orifice nozzle, beyond which the enhancement in the jet impulse production cannot be augmented further.

Another striking feature of the jet hydrodynamic impulse as the diameter ratio increases is the greater rise and drop of I_h^* at the onset and termination of the jet ejection, respectively. As shown in Fig. 7, for the tube nozzle case ($R_D = 1$), its hydrodynamic impulse rises rapidly during the initial acceleration while drops slightly during the jet deceleration ($t^* \approx 5$). On the other hand, for the orifice nozzle cases ($R_D > 1$), the magnitudes of these initial and final impulse fluctuation are amplified remarkably as the diameter ratio increases. The greater drop in I_h^* during jet termination for the orifice nozzle has also been observed in James and Madnia³² (see runs 1 in Fig. 15 therein). They suggested that the drop in the hydrodynamic impulse should be attributed to the formation of stopping vortices as well as the vertical wall boundary in the orifice cases. However, no further analysis on these two mechanisms was provided in their study. Unlike the effects of R_D on the total hydrodynamic impulse, which becomes levelled-off beyond the critical value $R_{D_cir} \approx 2$, the influence of R_D on the initial and final impulse variation is found to keep intensifying up to the

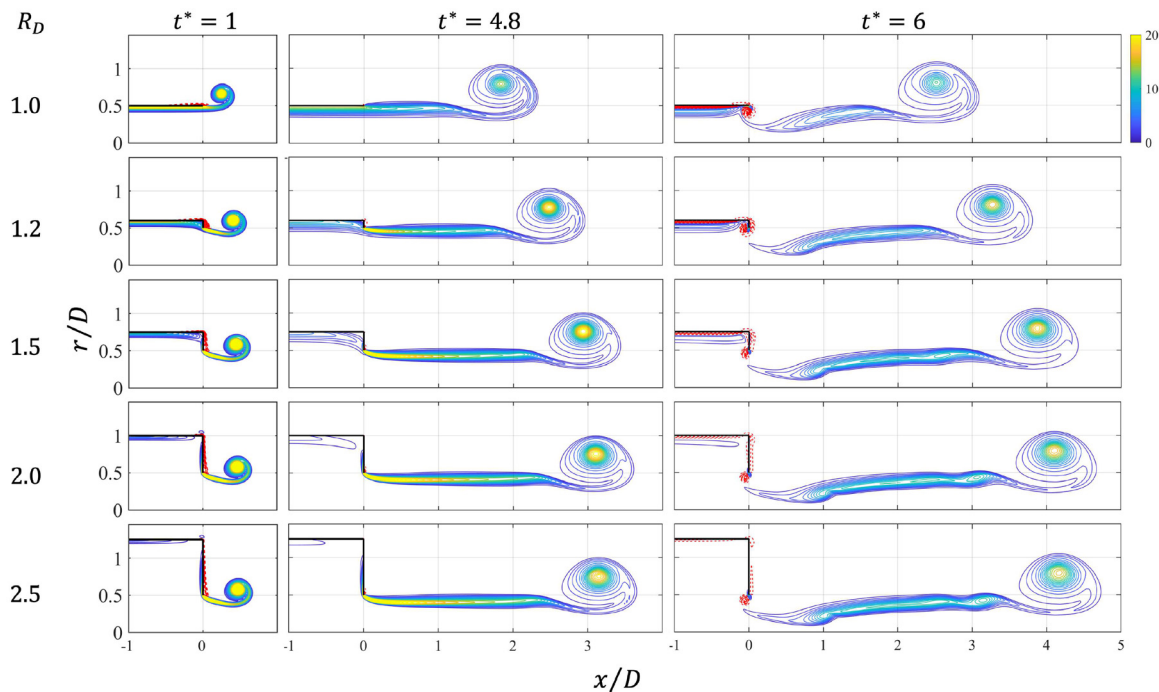


FIG. 8. Evolution of the vorticity contours for the jet from the tube and orifice nozzles. The minimum absolute contour level shown is $|\Omega| = 1$, and the increment is $\Delta\Omega = 1$. The red dashed lines indicate the negative vorticity levels.

maximum value of $R_D = 4$ studied here. Moreover, after its initial rise during the jet acceleration stage, the production of hydrodynamic impulse is first weakened and then rise again slowly. It approaches a constant rate of increase when entering the steady discharging stage. Similarly, the sudden drop in the hydrodynamic impulse during the jet deceleration stage is followed by a gradual recovery to the value prior to the sudden drop. It implies that the influence of the unsteady jet ejection is essentially transient and is restricted to a relatively short period of time after the acceleration and deceleration stages. As shown in Fig. 7, the influence of the diameter ratio on the initial and final I_h^* variation damps out after the jet enters the steady discharging stage and after the jet sets to rest, respectively. Therefore, the hydrodynamic impulse delivered by a single jet pulse depends primarily on its increase rate during the steady discharging stage, rather than on its transient variation related to the unsteady jet acceleration and deceleration.

To illustrate clearly the effects of the nozzle diameter ratio on the jet impulse generation, we plot the total hydrodynamic impulse per jet pulse I_{ht}^* (i.e., the value of I_h^* at $t^* = 15$) and the steady thrust T^* , normalized by the corresponding values for the classic slug model $I_{ht_SM}^*$ and T_{SM}^* , respectively, against the jet diameter ratio R_D in Fig. 9. Here, the steady thrust $T^* = (I_h^*)/(dt^*)$ is defined as the slope of the hydrodynamic impulse curves during the steady discharging stage. As shown, the total hydrodynamic impulse per jet pulse rises rapidly with the diameter ratio increasing from $R_D = 1$, while gradually levels off with time for $R_D \geq 2$. Moreover, it is found that the total hydrodynamic impulse and its steady increasing rate T^* approximately collapse on the same curve against the diameter ratio. This consolidates the aforementioned finding that the impulse generated during the steady discharging stage dominates the total hydrodynamic impulse

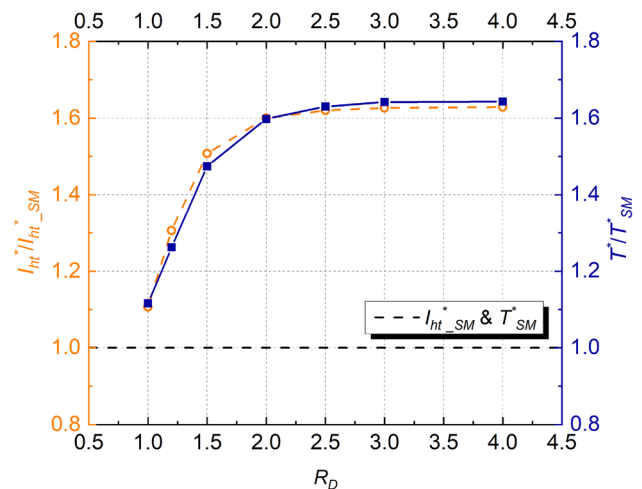


FIG. 9. The variation of the total hydrodynamic impulse and its steady increasing rate against the nozzle diameter ratio. Both data are normalized in terms of their values for the slug model, as shown by the horizontal dashed line.

generation, and the influence of the unsteady acceleration and deceleration of the jet becomes secondary.

B. Control volume analysis on the impulse in the jet wake

To reveal the underlying mechanisms for the development of the propulsive quantities at different diameter ratio, the components of

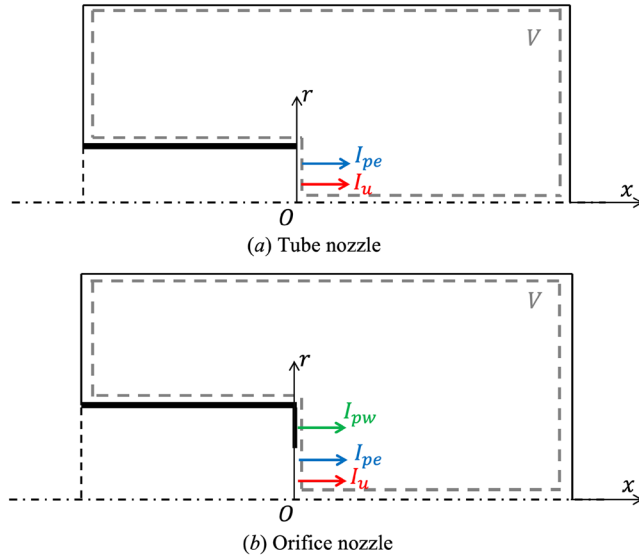


FIG. 10. The sketch of the control volume analysis for (a) the tube nozzle and (b) the orifice nozzle. The distribution and direction of the impulse terms in Eq. (3) are also shown schematically.

hydrodynamic impulse are to be investigated further. The hydrodynamic impulse I_h can be regarded as the jet impulse I_j supplied to the wake flow field through the jet exit. Adopting a control volume analysis in the near wake of the jet as shown schematically in Fig. 10 (see Olcay and Krueger²⁹), the jet impulse can be decomposed into the momentum flux term I_u and the pressure term I_p , as,

$$I_h(t) = I_j(t) = I_u(t) + I_p(t) = I_u(t) + I_{pe}(t) + I_{pw}(t), \quad (3)$$

where

$$I_u(t) = \rho \int_0^t \int_{A_{\text{exit}}} u_0^2(r, \tau) dS d\tau, \quad (4)$$

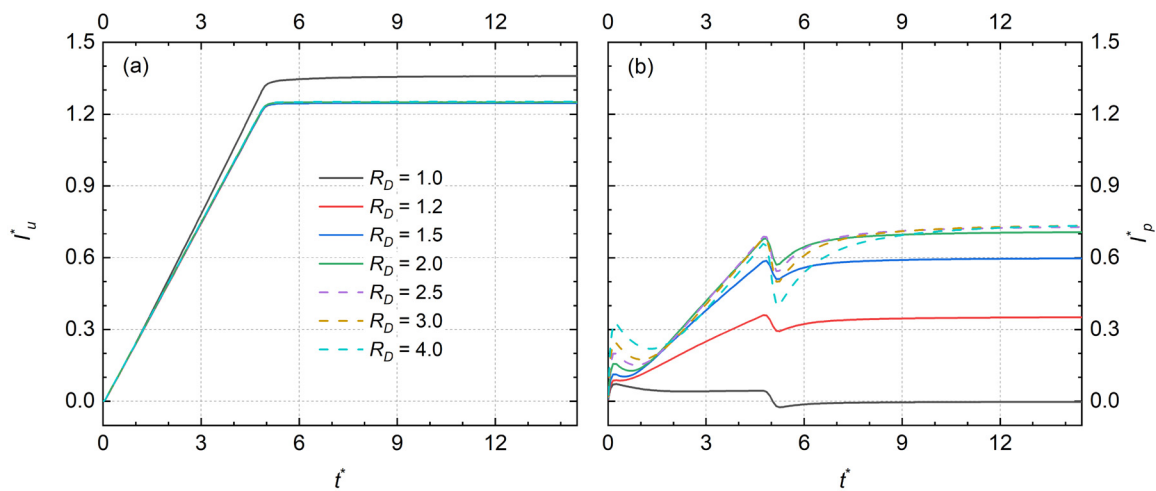


FIG. 11. The time histories of (a) the impulse due to momentum flux at the jet exit and (b) the pressure impulse with different diameter ratios.

$$I_{pe}(t) = \int_0^t \int_{A_{\text{exit}}} [p_0(r, \tau) - p_\infty] dS d\tau, \quad (5)$$

$$I_{pw}(t) = \int_0^t \int_{A_{\text{wall}}} [p_0(r, \tau) - p_\infty] dS d\tau. \quad (6)$$

For the orifice nozzle configuration, an additional term I_{pw} emerges due to the existence of the vertical wall on the exit plane, as illustrated in Fig. 10(b). It has been shown previously for the tube nozzle case that the hydrodynamic impulse in the jet wake is equal to the summation of the impulse supplied by the jet momentum I_u and that due to nozzle exit pressure I_{pe} .³⁰ Theoretically, this relationship can also be applied to the orifice nozzle cases studied here. Thus, given the validity of Eq. (3), the focus hereafter in this section will then be placed on the evolution of the three components of the jet impulse.

The evolutions of momentum flux term and pressure term of the jet impulse are presented in Fig. 11, in which the overall pressure impulse I_p is presented, instead of showing its exit and wall components separately. First, it is interesting to observe in Fig. 11(a) that the momentum flux contribution to jet impulse is actually higher for the tube nozzle than that for the orifice nozzles. This may be explained by the different velocity profile at the jet exit for these two configurations. The axial velocity for the flow issuing from tube nozzles has been studied extensively, which is characterized by the boundary layer growth inside the tube nozzle leading to higher velocity near the jet centerline and asymptotically approaching a parabolic profile as the jet proceeds.^{15,24,33,34} On the other hand, there is a minimum boundary layer development for the orifice nozzle cases throughout the jetting process, and the axial velocity is more uniformly distributed with minor peaks at the edge of the jet exit.^{25,27} Moreover, the momentum flux term remains unchanged as the diameter ratio increases for all the orifice nozzle cases, indicating that the diameter ratio has negligible influence on the axial velocity profile for the orifice nozzle jet.

Contrary to the insensitivity of the momentum flux term in the orifice nozzle regime, the pressure impulse exhibits conspicuous dependence on the diameter ratio as shown in Fig. 11(b). For the tube nozzle case, it has been found previously that the pressure impulse

varies appreciably only during the acceleration and deceleration phases,³⁵ due to the rapid change in jet velocity as well as the formation of the leading and stopping vortices.³⁰ Moreover, the pressure terms contribute negligibly to the total jet impulse as its final value at $t^* = 15$ is almost zero. For the orifice nozzle cases, Fig. 11(b) shows that the diameter ratio seems to have two noticeable effects on the pressure impulse production. First, it is observed that the growth rate of the pressure impulse rises more rapidly as the diameter ratio increases until a critical value of $R_{D_crit} \approx 2$ is approached, especially during the steady discharging stage. As a result, the pressure impulse makes a significant contribution (up to approximately 40%) to the total jet impulse for the orifice nozzle cases with large diameter ratio, in sharp contrast to the trivial total pressure impulse contribution for the tube nozzle case ($R_D = 1$). Second, as the diameter ratio increases, there appears greater variation of the pressure impulse during the jet acceleration and deceleration stages. Unlike the total pressure impulse at large formation time that becomes asymptotic beyond $R_D > 2.0$, the magnitude of the pressure impulse variation continues to intensify up to $R_D = 4.0$. However, the variation decays gradually after the acceleration and deceleration stages. One can see that the dependence of pressure impulse for a single pulse on R_D shows similar trend as that of hydrodynamic impulse against R_D as presented in Fig. 7. In short, one can see that the augmentation in the jet impulse for the orifice nozzle cases should be due largely to the pressure contribution at the jet exit plane, which persists throughout the jet ejection period, as indicated in Rosenfeld *et al.*²⁴ However, it may be pertinent to point out that the pressure rise occurs for the orifice nozzle cases should not be caused by the added mass effect due to jet acceleration or the influence of the initial vortex ring formation because these two factors exist only transiently after jet initiation.^{18,30}

Given the fact that large influence of the pressure contribution for the orifice nozzle configuration exists, we investigate further its characteristics by separating it into the jet-exit part and the vertical wall part. As shown in Fig. 10(b), the vertical plate at jet exit serves as a solid boundary of the control volume and, thus, would exert horizontal force to the fluid region considered. As a result, an additional term I_{pw} would emerge for the orifice nozzle configuration. The transient

development of the jet exit pressure impulse I_{pe} and wall pressure impulse I_{pw} is presented in Fig. 12 for the cases studied here. As shown in Fig. 12(a), the exit pressure impulse grows almost linearly after the initial jet acceleration, and its increase rate is enhanced by the larger diameter ratio up to about $R_D = 2.0$, similar to the diameter ratio dependence of I_j and I_p . There also exists abrupt rise and drop in I_{pe} at the onset and termination of the jet ejection phase, respectively, whose hydrodynamic mechanism had been explained previously in terms of the rapid jet velocity change.³⁰ It is interesting to observe that the magnitude of change in I_{pe} is almost independent of the diameter ratio, verifying that its origin is not linked to the jet nozzle geometry. On the other hand, Fig. 12(b) indicates that larger diameter ratio results in stronger variation of the wall pressure impulse during the jet acceleration and deceleration stages. As pointed out earlier, the wall pressure impulse variation would damp out rapidly after the unsteady acceleration and deceleration stages, indicating the temporally restricted influence of the orifice wall. Noting that the final value of I_{pw} at about $t^* = 15$ is actually negative for all orifice cases and diminishes further slightly as the diameter ratio increases. By examining the characteristics of these two pressure impulses components, we can conjecture that the augmentation of the jet impulse as the diameter ratio increases should stem from the jet exit pressure contribution I_{pe} , while the wall components of the pressure impulse I_{pw} are mainly responsible for the transient variation in the jet impulse during the initial acceleration and final deceleration stages, especially for the large diameter ratio cases.

C. Analysis on effects of jet nozzle diameter ratio

As pointed out by Krueger,²² the flow issuing from an orifice nozzle is very different from a tube nozzle owing to the fact that large contraction would be experienced by the flow as it approaches the jet exit, and that the flow would be restricted by the vertical wall boundary after it exits. The effects of nozzle diameter ratio on the propulsive characteristics of the single-pulsed jet, thus, can be examined in terms of these two mechanisms. The focus in this subsection will be placed on the characteristics of the pressure impulse terms (both I_{pe} and I_{pw}) because the momentum flux term has been shown to be unaffected by

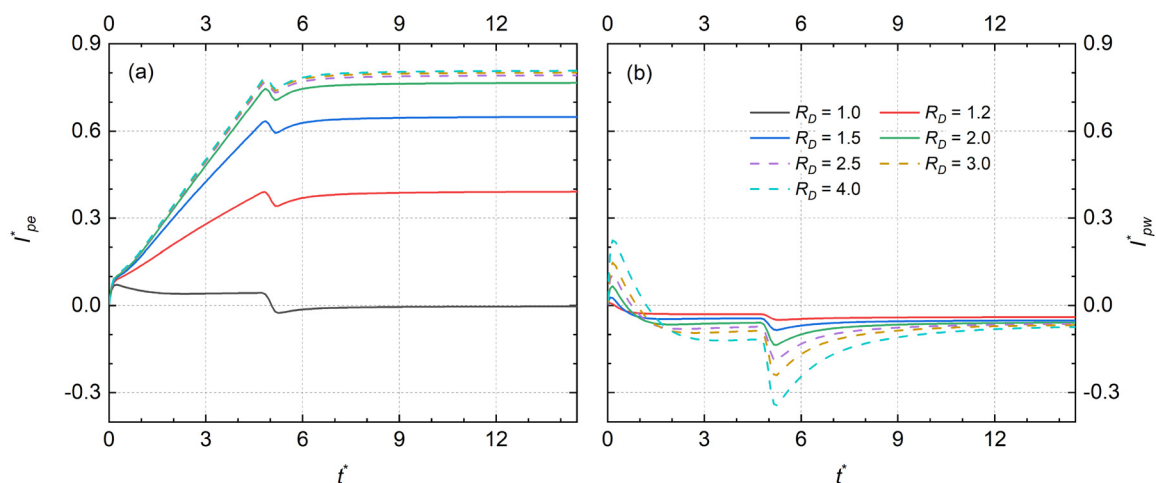


FIG. 12. The decomposition of the pressure impulse into (a) the jet exit term I_{pe} and (b) the vertical wall term I_{pw} for the single-pulsed jet with different diameter ratios.

the change in the diameter ratio for the orifice cases, as shown in Fig. 11(a).

For a steady jet, when fluid is discharging through an orifice, the flow would continue to contract over a short distance beyond the exit until the *vena contracta* is reached, as illustrated in Fig. 13. The resulting streamlines at the orifice exit plane indicate the existence of a transverse pressure gradient, which is believed to have contributed to the pressure impulse term at the exit I_{pe} . For the unsteady single-pulsed jet considered in the present study, the effect of flow contraction would become dominant during the steady discharging stage. The extent of flow contraction for the orifices of different diameter ratio is commonly characterized by the contraction coefficient C_c , defined as the ratio of the area of the reduced jet cross-sectional area at *vena contracta* A_{vc} to the jet exit area A , i.e., $C_c = A_{vc}/A$. Finding the contraction coefficient of a jet flow is a classical hydrodynamics problem, which was solved by Kirchhoff³⁶ and Von Mises³⁷ for a two-dimensional slit and by Trefftz³⁸ for an equivalent circular hole in an infinite plane. Rouse and Abul-Fetouh³⁹ suggested that jet profile for the axisymmetric case differs appreciably from that for the two-dimensional case, but the contraction coefficients are similar. Therefore, as suggested in the analysis of Limbourg and Nedić,²⁸ the theoretical result of Von Mises³⁷ will be used in the present work to estimate the contraction coefficients of axisymmetric jets exiting orifices, given as

$$C_c = \frac{D_0}{D} \sqrt{h} = R_D \sqrt{h}, \quad (7)$$

where h is a parameter fixing the upstream flow speed and can be solved from the equation

$$\left[\frac{2}{\pi} (1-h) \arctan \sqrt{h} + \sqrt{h} \right] = \frac{1}{R_D}.$$

The contraction coefficients for the orifice and tube nozzles are presented in Table II. For the orifice nozzle, the higher the diameter ratio is, the smaller the contraction coefficient becomes. The contraction coefficient is at about 0.64 when the diameter ratio reaches the critical value of $R_{D_crit} \approx 2.0$, which is close to the value adopted in Krueger,²³ i.e., 0.61 for $R_D \rightarrow \infty$.

The contribution of flow contraction to the jet impulse can be modeled by using a quasi-one-dimensional flow approximation with

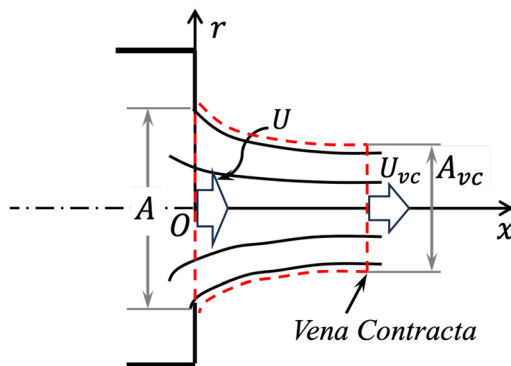


FIG. 13. Schematic of *vena contracta* for an orifice and the downstream area under consideration.

TABLE II. The contraction coefficient of the orifice nozzle cases.

R_D	1.0	1.2	1.5	2.0	2.5	3.0	4.0
C_c [Eq. (7)]	1.0	0.738	0.678	0.644	0.631	0.625	0.619

variable cross-sectional area from the nozzle exit to the *vena contracta*, as highlighted by the red dashed lines in Fig. 13. Applying mass and momentum conservation laws to the quasi-one-dimensional jet between the exit plane and the *vena contracta* and assuming that the pressure at the *vena contracta* is equal to ambient pressure p_∞ , the pressure p at the jet exit can be estimated as

$$p - p_\infty = \rho U^2 \left(\frac{1}{C_c} - 1 \right). \quad (8)$$

The expression for the thrust at the jet exit T_e (or equivalently, the time rate of jet exit pressure impulse plus the momentum flux at the exit) can then be estimated

$$T_e = \frac{d(I_{pe} + I_u)}{dt} = (p - p_\infty)A + \rho AU^2 = \frac{\rho AU^2}{C_c}. \quad (9)$$

The thrust at the jet exit obtained from the present numerical simulation and that predicted by the theoretical model of Eq. (9) is compared in Fig. 14. As shown, the theoretical results show good agreement with those from the present numerical simulation, with slight overprediction of the jet exit thrust at small diameter ratio cases (i.e., $R_D = 1.2, 1.5$). The relative error between the values calculated by the theoretical model and the numerical values does not exceed 10% for all the cases.

As discussed in Sec. III B, the greater variation of the jet impulse during the onset and end of the ejection phase as the diameter ratio increases can be attributed to the greater pressure forces acting on the vertical wall. The effect of the vertical exit wall of nozzle on the jet

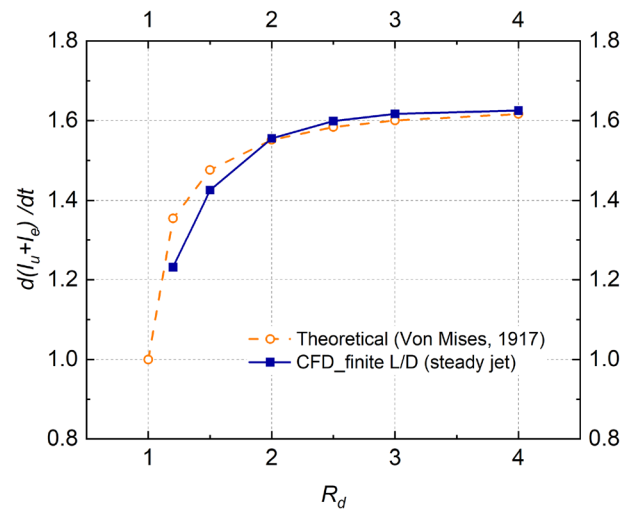


FIG. 14. Comparison of the results of the time rate of the pressure impulse at the nozzle exit from Eq. 9 and the present numerical simulation. The data are normalized by the slug model prediction of I_{pe} for the tube nozzle case, i.e., $\pi \rho (D/2)^2 U^2$.

dynamics has been studied previously, for example, by James and Madnia³² and Gharib *et al.*¹⁷ It should be noted that in those previous studies, the nozzle geometry is neither the tube nozzle nor the orifice nozzle configurations as used in the current study. Instead, it consists of a vertical plate flushed mounted with the exit of a straight tube. As a result, the flow upstream of the jet exit plane is almost parallel, i.e., similar to that for a tube nozzle case. Nonetheless, the flow will be affected by the wall boundary at the exit plane after discharging, similar to that for an orifice nozzle case. James and Madnia³² found that the presence of the vertical plate would decrease the total jet impulse further during the jet termination, relative to the tube nozzle case with the identical flow conditions. Gharib *et al.*¹⁷ studied the jet issuing out of a tube nozzle with a vertical wall installed at its exit plane and obtained that the vortex ring circulation decreased slightly owing to the opposite-sign vorticity generated the secondary boundary layer on the outside wall.

As shown in Eq. (6), the wall pressure term of the jet impulse I_{pw} is determined by both temporal and spatial distributions of the pressure on the outside wall. To account for the change in I_{pw} at different diameter ratio, the evolution of the pressure field near the jet exit for three orifice nozzle cases at five instants is presented in Fig. 15. The most striking feature one can observe is that, given the obvious difference in nozzle geometry, the pressure distributions in the near wake (i.e., downstream of the jet exit plane) at each instant are qualitatively similar for the three cases, especially for the cases $R_D = 2.0$ and $R_D = 4.0$. During the initial acceleration stage (at $t^* = 0.153$, as shown in the first column of Fig. 15), a negative pressure region is formed just downstream of the lip of the orifice, which is induced by the forming vortex ring. It can be seen that the size and shape of the pressure distributions for the three cases are roughly identical, except that the induced negative pressure region has extended to the outer

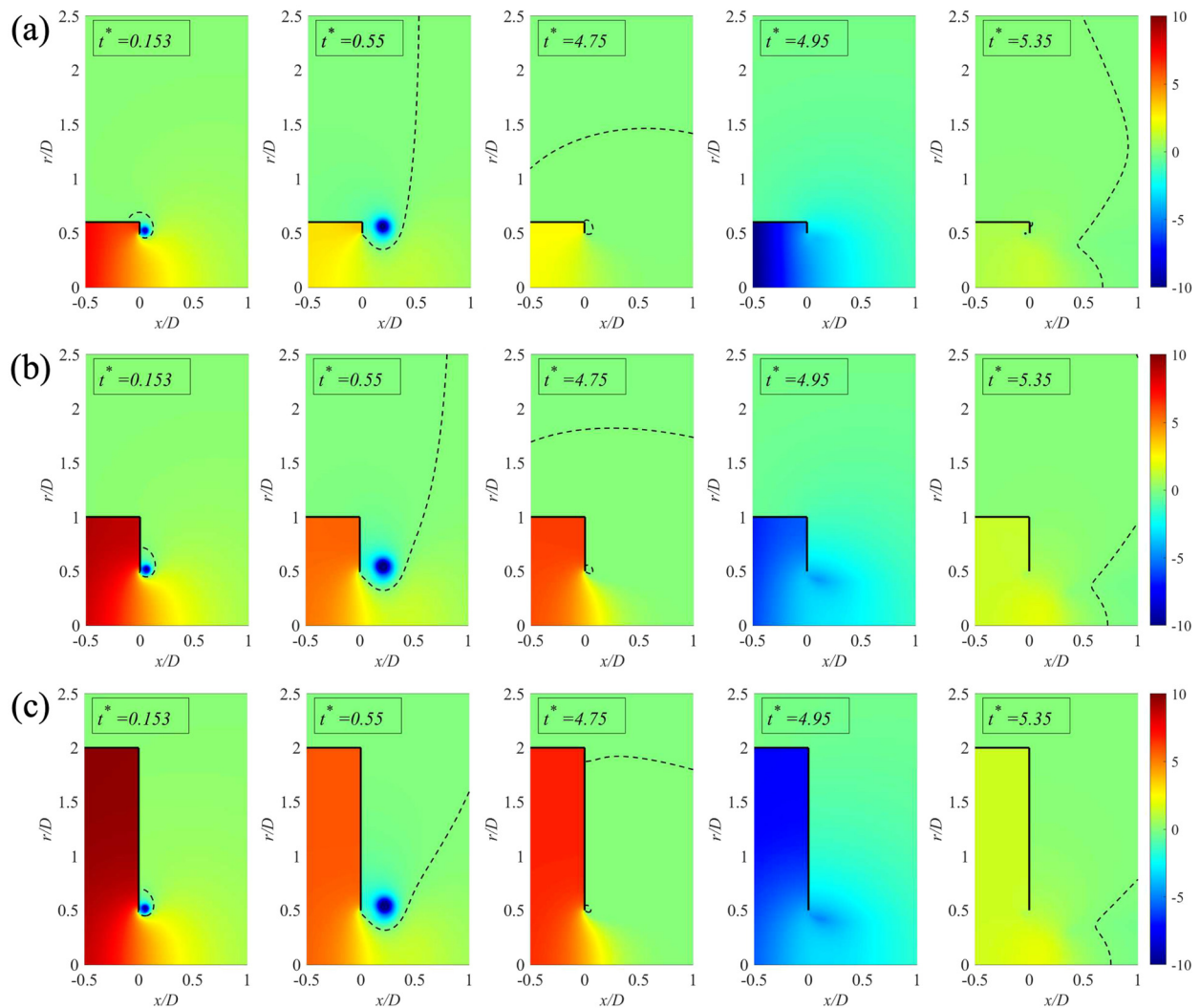


FIG. 15. Evolution of the pressure field in the region around the jet exit for the entire jet ejection period for the orifice nozzle cases (a) $R_D = 1.2$, (b) $R_D = 2.0$, and (c) $R_D = 4.0$. The black dashed line indicates the contour line of zero pressure coefficient.

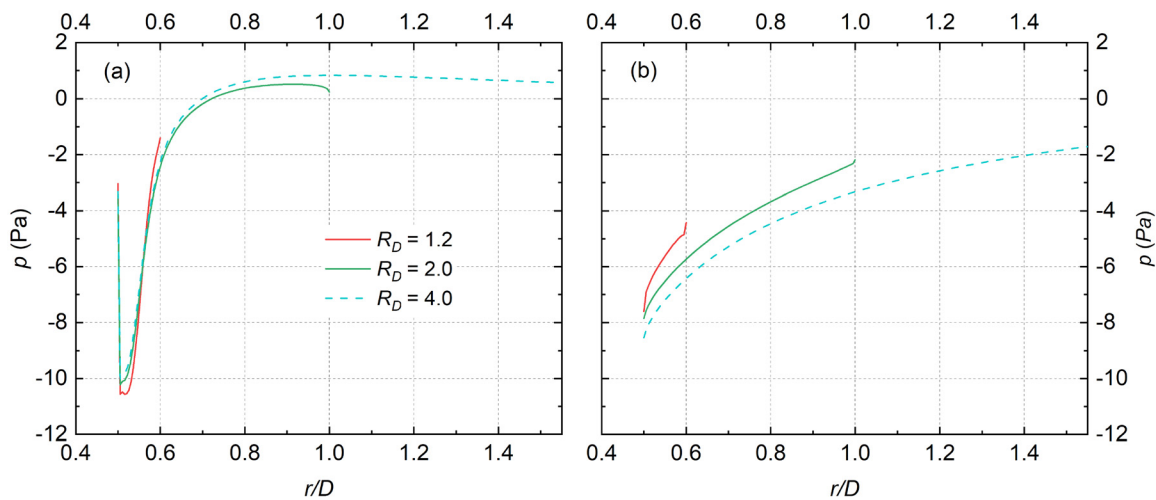


FIG. 16. The distribution of pressure coefficient on the vertical wall of the orifice nozzle for different diameter ratio at (a) $t^* = 0.153$ and (b) $t^* = 4.95$.

boundary of the cylindrical nozzle for case $R_D = 1.2$ due to a smaller size of the vertical wall. Similar situations can also be observed for the following instants presented in Fig. 15. This feature is further verified by the distribution of the pressure over the vertical wall at two instants during the acceleration and the deceleration stages, as shown in Fig. 16. Based on the aforementioned observation, one can speculate that the diameter ratio, as well as the flow contraction, should have negligible effect on the pressure distribution in the jet near wake, specifically on the outside vertical wall. Consequently, greater variation of I_{pw} during the onset and end of the jet ejection phase as the diameter ratio increases should be associated with the larger area of the vertical wall for the greater diameter ratio cases.

To further verify the dominant influence of vertical wall area on the wall pressure term of the jet impulse, we adopt a modified geometric configuration of the orifice nozzle (labeled as $R_D = 1.2b$ to $R_D = 3.0b$), as shown schematically in Fig. 17. These cases have the same nozzle internal geometry as the original orifice nozzle cases, but the area of the vertical wall is kept the same as that for the case O4.0 ($R_D = 4.0$). In other words, the outside wall boundary is identical for all modified orifice nozzles, but the internal flow contraction effect varies as the diameter ratio changes. This modified jet configuration serves to decouple the influence of flow contraction near the jet exit and the effect of the vertical wall boundary.

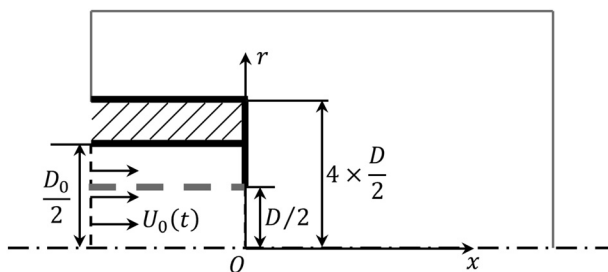


FIG. 17. Geometry of the modified configuration of the orifice nozzle with the same internal diameter ratio as the first configuration. The vertical wall area is the same as that for case O4.0 with diameter ratio $R_D = 4.0$.

The evolution of two components of the pressure impulse, i.e., the jet exit term I_{pe} and the vertical wall term I_{pw} , for the modified orifice nozzle cases as well as orifice case O4 is presented in Fig. 18. Comparing Fig. 18(a) with Fig. 12(a), one can see that the magnitude and variation of jet exit pressure term I_{pe} do not exhibit any significant differences for the cases with the same diameter ratio. For Fig. 18(b), it shows that, despite with the different diameter ratio, the wall pressure terms I_{pw} approximately collapse on a single curve for all cases. Given the same vertical wall boundary condition for all the modified orifice nozzle cases, the results, thus, imply that the effect of the vertical wall on the jet impulse generation is determined primarily by its area, while the flow contraction near the jet exit has negligible effect on the wall pressure term.

To further analyze the characteristics of the wall pressure impulse I_{pw} for different diameter ratio cases, we propose two quantities, i.e., its initial rise during the jet onset ΔI_{rise} and its sudden drop during the jet termination ΔI_{drop} to determine the variation of I_{pw} . As illustrated in Fig. 18(b), ΔI_{rise} is defined as the difference between the maximum of I_{pw} and its initial value at the beginning (i.e., zero value), and ΔI_{drop} is defined as the difference between the value of I_{pw} right before the jet deceleration (i.e., at $t^* = 4.75$ for the present velocity program) and its minimum value. The dependence of the variation of the wall pressure impulse on the diameter ratio for the two types of orifice nozzle configurations is presented in Fig. 19. It clearly shows that for all cases of the modified orifice nozzle, the magnitudes of the wall pressure impulse rise and drop are nearly the same, equal to the original orifice nozzle case O4 with $R_D = 4.0$ with the same vertical wall area, except slightly higher value for the small diameter ratio cases. Moreover, for the original orifice nozzle cases, the magnitude of wall pressure impulse variation is found to increase almost linearly with the diameter ratio. Given the negligible influence of the jet flow contraction on the wall pressure distribution, it substantiates our early conjecture that the greater variation of I_{pw} during the onset and the end of the ejection phase as the diameter ratio increased is the consequence of the larger vertical wall area for the greater diameter ratio cases. Finally, it is worth noting that our interpretation of the effect of the diameter ratio on the jet impulse production in terms of the flow contraction as well as the vertical wall

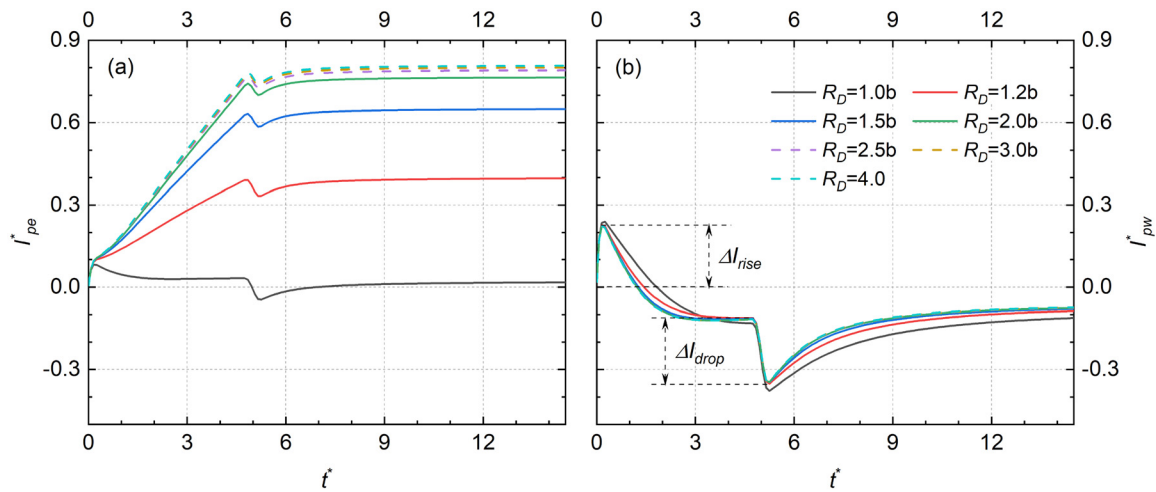


FIG. 18. The evolution of the pressure impulse components for the single-pulsed jet with the modified orifice nozzle configuration. (a) The jet exit term I_{pe} and (b) the vertical wall term I_{pw} .

boundary can satisfactorily account for the asymptotic feature of the total jet impulse when the diameter ratio increases beyond the critical value of $R_{D_c} \approx 2$, and for the ever increasing of the jet impulse variation magnitude during the onset and end of the jet ejection phase up to $R_D = 4$.

IV. CONCLUDING REMARKS

The transient development of the impulse and thrust generated by single-pulsed jets from different nozzle configurations has been studied numerically to elucidate the influence of the nozzle diameter ratio $R_D = D_0/D$ on the propulsive characteristics of the jets. Unlike most previous studies,^{24,28} the different nozzle geometric configurations considered in the present study have the identical jet exit conditions by setting the jet exit diameter D invariant while changing the nozzle diameter D_0 , so as to concentrate exclusively on the effects of

the diameter ratio. The results of the hydrodynamic impulse indicate that the nozzle geometry at the jet exit has significant influence on the propulsive characteristics of the single-pulsed jet during its entire ejection phase. The single-pulsed jet discharged from the orifice nozzles ($R_D > 1$) delivers greater total impulse into its wake than the tube nozzle ($R_D = 1$). For the orifice nozzles, the impulse production is augmented as the diameter ratio increases until a critical value of $R_{D_crit} \approx 2.0$ is approached. Through a control volume analysis encompassing the near wake of the jet, we found that, although the momentum flux component I_u is slightly weaker for the orifice nozzle configuration, the positive and sustained contribution from the jet exit pressure term I_{pe} leads to the larger total impulse production. In addition, the wall pressure term I_{pw} serves primarily to cause the transient variations in the jet impulse during the onset and end of the jet ejection phase as the diameter ratio increases. Moreover, the final value I_{pw} for a single jet pulse is found to be negative for all the diameter ratios considered, in contrast to the obvious positive contribution from the jet exit over-pressure term I_{pe} .

The influence of jet nozzle diameter ratio on the propulsive characteristics of the single-pulsed jets is interpreted in terms of the flow contraction at the jet exit as well as the flow restriction by the vertical wall. The greater radial velocity at the jet exit caused by the flow contraction effect is responsible for the augmented growth rate of the pressure impulse as the diameter ratio increases, especially during the steady discharging stage. By adopting the contraction coefficient C_c to parameterize quantitatively the extent of the flow contraction, a theoretical model has been developed under the quasi-one-dimensional flow approximation to predict the pressure thrust at the jet exit, showing good agreement with the present numerical results. On the other hand, the transient variation of the jet impulse during the acceleration and deceleration stages is found to be attributed to the pressure forces acting on the outside of the vertical wall. The snapshots of the pressure field in the near wake show that the pressure distributions on the vertical wall are actually insensitive to the change in the nozzle diameter ratio, which, in turn, indicates that the greater transient variation of the jet impulse as R_D increases is primarily associated with the change in the vertical wall area.

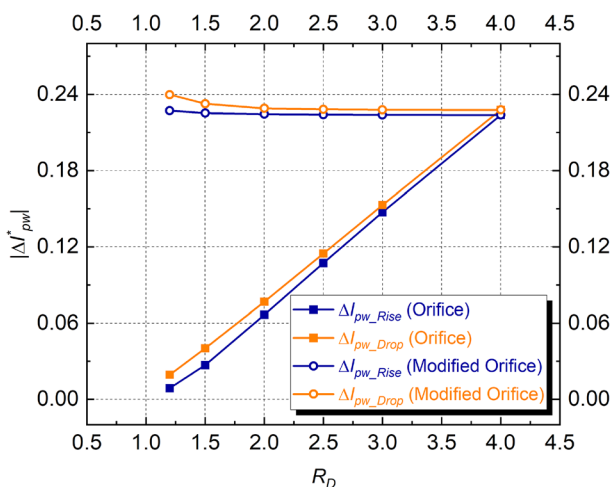


FIG. 19. The variation of the fluctuation magnitude of the wall pressure impulse against the nozzle diameter ratio for the original and modified orifice nozzle cases.

The effects of flow restriction by the vertical wall by means of its area are further verified by comparing the magnitudes of pressure impulse variation between the two orifice nozzle configurations with the different vertical wall area at the same diameter ratio.

Finally, the results of the present study may offer a simple design principle for the augmentation of the impulse and thrust production of the unsteady pulsed jet with static orifice nozzle geometry in practical applications, such as the pulsatile aquatic propulsion for unmanned underwater vehicles (UUV). It is shown here that by using the orifice nozzles, the single-pulsed jet is capable of generating larger impulse to its wake as the diameter ratio increases. However, this effect saturates asymptotically after the diameter ratio becomes larger than the critical value of $R_{D_cri} \approx 2$. It suggests that, using the orifice nozzle generator with the diameter ratio beyond $R_{D_cri} \approx 2$ would not provide appreciable benefit of impulse augmentation but cause undesired thrust fluctuation during the jet period. Therefore, in addition to the previously established advantages of unsteady pulsed jet for propulsion,^{11,18,30} the present results imply further that the propulsive performance can be optimized by the orifice nozzle configuration with its diameter ratio close to the critical value of two.

AUTHOR DECLARATIONS

Conflict of Interest

The authors have no conflicts to disclose.

Author Contributions

Lei Gao: Data curation (lead); Formal analysis (lead); Funding acquisition (equal); Methodology (equal); Resources (equal); Validation (equal); Writing – original draft (equal); Writing – review & editing (equal). **Xin Wang:** Data curation (equal); Formal analysis (supporting); Investigation (lead); Validation (equal); Writing – original draft (equal). **Simon C. M. Yu:** Funding acquisition (equal); Methodology (equal); Resources (equal); Supervision (lead); Writing – review & editing (equal).

DATA AVAILABILITY

The data that support the findings of this study are available from the corresponding author upon reasonable request.

REFERENCES

- D. Weihs, "Periodic jet propulsion of aquatic creatures," *Fortschr. Zool.* **24**, 171–175 (1977).
- P. S. Krueger and M. Gharib, "Thrust augmentation and vortex ring evolution in a fully-pulsed jet," *AIAA J.* **43**, 792–801 (2005).
- R. W. Whittlesey and J. O. Dabiri, "Optimal vortex formation in a self-propelled vehicle," *J. Fluid Mech.* **737**, 78–104 (2013).
- B. J. Gemmell, J. O. Dabiri, S. P. Colin, J. H. Costello, J. P. Townsend, and K. R. Sutherland, "Cool your jets: Biological jet propulsion in marine invertebrates," *J. Exp. Biol.* **224**, jeb222083 (2021).
- T. L. Daniel, "Mechanics and energetics of medusan jet propulsion," *Can. J. Zool.* **61**, 1406–1420 (1983).
- J. H. Costello, S. P. Colin, J. O. Dabiri, B. J. Gemmell, K. N. Lucas, and K. R. Sutherland, "The hydrodynamics of jellyfish swimming," *Annu. Rev. Mar. Sci.* **13**, 375–396 (2021).
- E. J. Anderson and M. E. Demont, "The mechanics of locomotion in the squid *Loligo pealei*: Locomotory function and unsteady hydrodynamics of the jet and intramantle pressure," *J. Exp. Biol.* **203**, 2851–2863 (2000).
- C. A. York, I. K. Bartol, P. S. Krueger, and J. T. Thompson, "Squids use multiple escape jet patterns throughout ontogeny," *Biol. Open* **9**, bio054585 (2020).
- K. R. Sutherland and L. P. Madin, "Comparative jet wake structure and swimming performance of salps," *J. Exp. Biol.* **213**, 2967–2975 (2010).
- P. F. Linden and J. S. Turner, "Optimal vortex rings and aquatic propulsion mechanisms," *Proc. R. Soc. B* **271**, 647–653 (2004).
- J. O. Dabiri, "Optimal vortex formation as a unifying principle in biological propulsion," *Annu. Rev. Fluid Mech.* **41**, 17–33 (2009).
- N. W. Xu, "Squid-inspired robots perform swimmingly," *Sci. Rob.* **6**, eabf4301 (2021).
- Q. Zhu and Q. Xiao, "Physics and applications of squid-inspired jetting," *Bioinspiration Biomimetics* **17**, 041001 (2022).
- T. Maxworthy, "Some experimental studies of vortex rings," *J. Fluid Mech.* **81**, 465–495 (1977).
- N. Didden, "On the formation of vortex rings: Rolling-up and production of circulation," *Z. Angew. Math. Phys.* **30**, 101–116 (1979).
- A. Glezer, "The formation of vortex rings," *Phys. Fluids* **31**, 3532–3542 (1988).
- M. Gharib, E. Rambod, and K. Shariff, "A universal time scale for vortex ring formation," *J. Fluid Mech.* **360**, 121–140 (1998).
- P. S. Krueger and M. Gharib, "The significance of vortex ring formation to the impulse and thrust of a starting jet," *Phys. Fluids* **15**, 1271–1281 (2003).
- L. A. Ruiz, R. W. Whittlesey, and J. O. Dabiri, "Vortex-enhanced propulsion," *J. Fluid Mech.* **668**, 5–32 (2011).
- Q. Huang, F. B. Tian, J. Young, and J. C. S. Lai, "Transition to chaos in a two-sided collapsible channel flow," *J. Fluid Mech.* **926**, A15 (2021).
- D. I. Pullin, "Vortex ring formation at tube and orifice openings," *Phys. Fluids* **22**, 401–403 (1979).
- P. S. Krueger, "An over-pressure correction to the slug model for vortex ring circulation," *J. Fluid Mech.* **545**, 427–443 (2005).
- P. S. Krueger, "Circulation and trajectories of vortex rings formed from tube and orifice openings," *Physica D* **237**, 2218–2222 (2008).
- M. Rosenfeld, K. Katija, and J. O. Dabiri, "Circulation generation and vortex ring formation by conic nozzles," *J. Fluids Eng.* **131**, 091204 (2009).
- M. Krieg and K. Mohseni, "Modelling circulation, impulse and kinetic energy of starting jets with non-zero radial velocity," *J. Fluid Mech.* **719**, 488–526 (2013).
- R. Limbourg and J. Nedić, "Formation of an orifice-generated vortex ring," *J. Fluid Mech.* **913**, A29 (2021).
- R. Limbourg and J. Nedić, "An extended model for orifice starting jets," *Phys. Fluids* **33**, 067109 (2021).
- R. Limbourg and J. Nedić, "An extension to the universal time scale for vortex ring formation," *J. Fluid Mech.* **915**, A46 (2021).
- A. B. Olcay and P. S. Krueger, "Momentum evolution of ejected and entrained fluid during laminar vortex ring formation," *Theor. Comput. Fluid Dyn.* **24**, 465–482 (2010).
- L. Gao, X. Wang, S. C. M. Yu, and M. K. Chyu, "Development of the impulse and thrust for laminar starting jets with finite discharged volume," *J. Fluid Mech.* **902**, A27 (2020).
- K. Shariff and A. Leonard, "Vortex rings," *Annu. Rev. Fluid Mech.* **24**, 235–279 (1992).
- S. James and C. K. Madnia, "Direct numerical simulation of a laminar vortex ring," *Phys. Fluids* **8**, 2400–2414 (1996).
- M. Shusser, M. Gharib, M. Rosenfeld, and K. Mohseni, "On the effect of pipe boundary layer growth on the formation of a laminar vortex ring generated by a piston/cylinder arrangement," *Theor. Comput. Fluid Dyn.* **15**, 303–316 (2002).
- J. O. Dabiri and M. Gharib, "A revised slug model boundary layer correction for starting jet vorticity flux," *Theor. Comput. Fluid Dyn.* **17**, 293–295 (2004).
- X. Bi and Q. Zhu, "Pulsed-jet propulsion via shape deformation of an axisymmetric swimmer," *Phys. Fluids* **32**, 081902 (2020).
- G. Kirchhoff, "Zur theorie freier flüssigkeitsstrahlen," *J. Reine Angew. Math.* **70**, 289–298 (1869).
- R. von Mises, "Berechnung von Ausfluss und Überfallzahlen," *Z. Ver. Dtsch. Ing.* **61**, 447–452, 469–474, and 493–498 (1917).
- E. Trefftz, "Über die kontraktion kreisförmiger flüssigkeitsstrahlen," *Z. Math. Phys.* **64**, 34–61 (1916).
- H. Rouse and A. H. Abul-Fetouh, "Characteristics of irrotational flow through axially symmetric orifices," *J. Appl. Mech.* **17**, 421–426 (1950).